Int. J. Nano Dimens., 12 (1): 20-36, Winter 2021

ORIGINAL ARTICLE

Morphological investigation of Graphene Oxide/ Polyacrylamide super-elastic nanocomposite by a solution polymerization process with enhanced rheological property and thermal conductivity

Hosein Gudarzifar [1], ***Alireza Rezvani*** [1,*], ***Samad Sabbaghi*** [2,*]

[1]*Department of Chemistry, University of Sistan and Baluchestan, Zahedan, Iran*
[2]*Faculty of Advanced Technologies, Nano Chemical Engineering Department, Shiraz University, Shiraz, Iran*

Received 06 August 2020; revised 07 October 2020; accepted 08 October 2020; available online 10 October 2020

Abstract

TA series of Graphene Oxide/ Polyacrylamide (GO/PAM) super-elastic nanocomposites with different amounts of Graphene Oxide Nanosheets (GONSs) (0.5, 1, 1.5, and 2 wt. %) were synthesized using an in-situ polymerization in an aqueous medium in this paper. To this end, we proposed a method for obtaining super-elastic nanocomposites with a high dispersion of GONSs in the PAM chains as well as in a rapid synthesis. Fine adaptability, powerful inner interaction between embedded GONSs into the PAM chains, and remarkable enhancement of mechanical and thermal properties of synthesized GO/PAM super-elastic nanocomposites can be considered as the unique characteristics of this synthesis method in a short time. In this study, GONSs were prepared by a modified Hummer's procedure at ambient temperature. Fourier Transform Infrared (FT-IR) spectroscopy, X-Ray Diffraction (XRD), Field Emission Scanning Electron Microscopy (FESEM), thermo-Gravimetric Analysis (TGA) and Differential Thermal Analysis (DTA) were employed to characterize the internal network structure of GONSs, PAM, and GO/PAM nanocomposites. XRD investigation indicated the increase of the interlayer spacing of GONSs. The exfoliation and dispersion of GONSs in the PAM matrix were studied by XRD and FESEM. The formation of oxygen-including groups on the surface of GONSs and hydrogen linking between GONSs and PAM was confirmed by FT-IR spectra and DTA. Atomic Force Microscopy (AFM) was used to evaluate the thickness of the synthesized GONSs that was measured to be about 6.85 nm. Ultraviolet-Visible (UV/vis) spectroscopy illustrated the high percent of oxidation with more oxygen-including groups on the GONSs basal surface. Raman spectroscopy was also utilized to determine the induced disorder degree in the synthesized graphene oxide and distinguish the number of its layers. Thermal properties curves of GO/PAM nanocomposites represented an improvement trend in degradation temperature and a remaining amount up to GO-loaded (1.5 wt. %). The addition of GONSs also showed the significant improvement of viscoelastic behavior in PAM chains. The highest storage modulus (G'; 6.42 MPa) and loss modulus (G"; 0.98 MPa) are related to GO/PAM nanocomposite with 1.5 wt. % GO-loading. Based on the empirical result, the GONSs could remarkably enhance the thermal conductivity of PAM which was measured to be about 0.49 $W.m^{-1}.K^{-1}$. Thermal conductivity of $GO_{1.5}$/PAM nanocomposite was about 0.9 $W.m^{-1}.K^{-1}$ that showed 84 % increase compared to the PAM.

Keywords: *GONSs; GO/PAM Nanocomposite; Rheological Property; Solution Polymerization; Thermal Conductivity.*

How to cite this article

Gudarzifar H., Rezvani A.R., Sabbaghi S. Morphological investigation of Graphene Oxide/ Polyacrylamide super-elastic nanocomposite by a solution polymerization process with enhanced rheological property and thermal conductivity. Int. J. Nano Dimens., 2020; 12(1): 20-36.

* Corresponding Authors Email: *ali@hamoon.usb.ac.ir, sabbaghi@shirazu.ac.ir & samad.sabbaghi@uwaterloo.ca*

INTRODUCTION

The graphene is a flat single layer formed of sp^2-bonded carbon atoms ordered in a two-dimensional honeycomb structure. It has interested many researchers due to its special electrical, thermal, mechanical properties, and low density [1-5]. Graphene Oxide Nanosheets (GONSs) have excited major interest as additives to incorporate with other polymers [6-8] due to their great surface area [9-11]. GONSs have a sheet structure and are wealthy in oxygen-including groups, such as epoxy, carbonyl, and hydroxyl groups [12, 13]. It should be noted that the oxygen-including groups on the GONSs plane are very important for the synthesis of GO/polymer [14]. They simplify the dispersion of GONSs in aqueous solutions and provide reactive sites for the polymer growth through manufacturing hydrogen bonding with the polymer chain. For example, the oxygen-containing groups of the GONSs manufacture hydrogen bonding with the N-H bond of polyacrylamide (PAM).

GO was prepared in 1859 by Brodie via adding KCl (potassium chlorate) to a dispersed graphite in concentrated HNO_3 (nitric acid) [15]. It was also generated using different methods in which the Staudenmaier [16] or Hammer [17] procedures were improved to minimize the risk of explosion. In these methods, graphite was oxidized using powerful oxidants, such as $KMnO_4$ (Potassium permanganate), KCl, and $NaNO_3$ (sodium nitrate) in H_2SO_4 (sulfuric acid) or its mixture with HNO_3 or mixture of H_2SO_4 and H_3PO_4 (phosphoric acid) [18, 19]. This process, which generates oxygen-containing groups on the surface of graphite layers, has a significant effect on reducing van der Waals interaction between layers as well as increasing interlayer distances [20]. Actually, the irregularity of the graphite network is reflected in an increment of layers' distance to 0.335 nm for graphite and more than 0.825 nm for GO.

Several techniques have been employed to prepare polymer grafted GONSs, such as melt blending [21-24], solution mixing [25-27], and in-situ radical polymerization [28-34]. However, other methods have been also employed to disperse the GONSs in a polymer base, such as Atom Transfer Radical Polymerization (ATRP) [35-37], Reversible Addition Fragmentation chain Transfer process (RAFT) [38-40], Nitroxide Mediated Polymerization (NMP) [41, 42], and in-situ Free Radical Polymerization (FRP) [43, 44]. Among these methods, in-situ radical polymerization in aqueous is the simplest due to the fact that the other methods all require special reaction conditions. One of the advantages of this method is that it does not use any additional surfactant because GONSs can stabilize the emulsion or microemulsion polymerization of various monomers, like styrene and methyl methacrylate [45-47].

The presence of GONSs in the structure of polymers has made a remarkable enhancement in the mechanical, thermal, rheological, and electrical properties of polymer-based nanocomposites at very low filler content compared to the polymer-based composites synthesized with micron-scale fillers [48]. The GONSs content has not only significantly influenced the rheological behaviors but also improved the mechanical strength in GO/ polyacrylamide/ carboxymethyl cellulose sodium (GO/ PAM/ CMC) [49]. The intermolecular instructions between the components of GO/ poly (acrylic acid-g-acrylamide) (GO/poly (AA-g-AM)) have been effectively enhanced with lower content of GONSs that was dispersed in the polymer matrix [50]. P. Liu et al. demonstrated that the addition of GONSs enhanced the thermal and mechanical properties of polyimide [51]. Habib *et al.* indicated that the electrical and thermal properties of GO/ nitrile butadiene rubber (GO/ NBR) nanocomposite were enhanced compared to NBR without GO [52]. The addition of only a small amount of GONSs in the structure of polyethylene tetrasulfide (PSP) has also enhanced the thermal properties and the melting point [53]. Thomassin *et al.* prepared the GO/polymethylmethacrylate (GO/PMMA) nanocomposite and founded that the GONSs content in polymer structures led to an improvement in rheological properties [48]. Zhang et al. prepared GO/polyethyleneglycol as a reinforcing nanofiller of polylactic acid (GO/ PEG/PLA) and showed that both GO and GO/PEG enhanced the thermal properties of PLA, while GO/PEG was still more effective [54].

The current study investigates the synthesis of super-elastic nanocomposites with a high dispersion of GONSs in the PAM chains by solution polymerization in a short time. The influence of GONSs content on the expanse of its dispersion, thermal conductivity, rheological, and thermal properties of derived GO/PAM nanocomposites was also explored. GONSs were synthesized using an improved method which is not only extracted

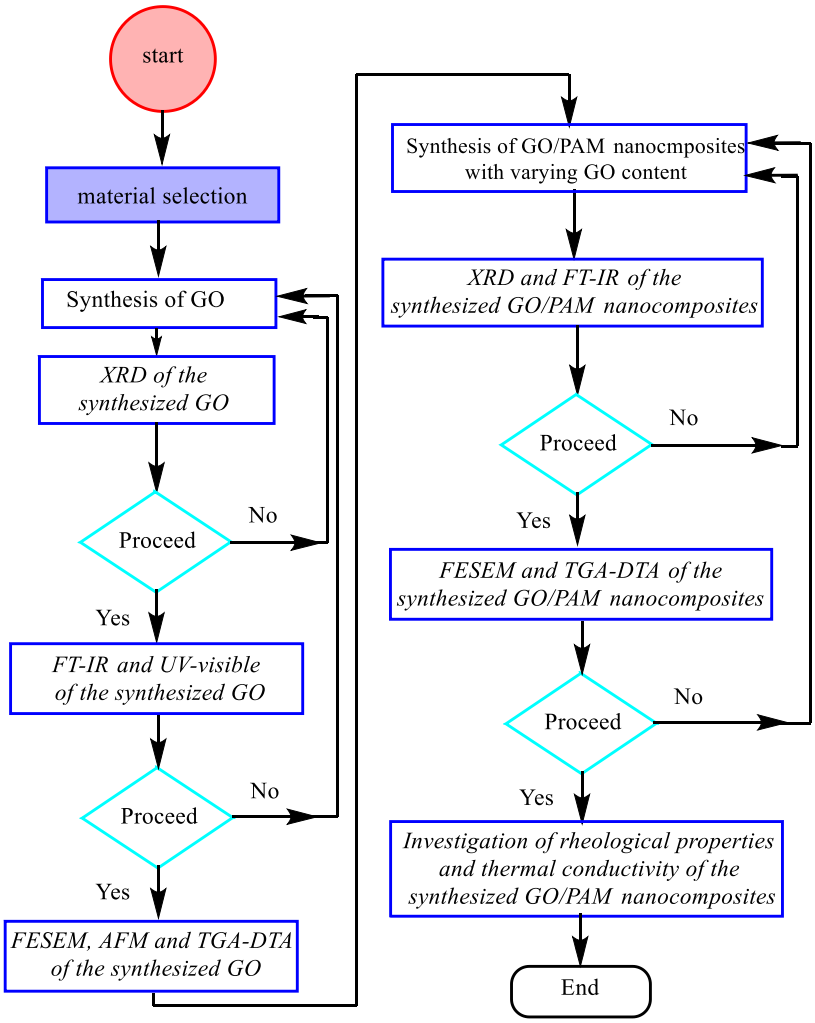

Fig. 1. Experimental procedure flowchart.

using Hammer's method, Staudeumaier's method, and Brodie's method but also is hassle-free of these methods. In this procedure, GONSs are simplified fabricated by increasing graphite flake and $KMnO_4$ into concentrated H_2SO_4 and H_3PO_4 under constant stirring. PAM is a water-soluble polymer with a large number of acetylamine functional groups on its chains that can interact with oxygen-activated groups of GONSs by chemical or physical adsorption, such as hydrogen bond interaction. Ren *et al.* demonstrated that PAM can be used as a stabilizer in preparing a graphene dispersion [55]. According to these reasons, it can be said that using PAM as the base polymer will reduce the agglomeration of GONSs and produce the GO/PAM nanocomposites with the fine dispersion of nanoparticle. GO/PAM nanocomposites with changing weight ratio (0.5, 1, 1.5, and 2 wt. %) of GONSs to the constant amount of acrylamide monomer (20 g) were prepared by a solution polymerization method. The flowchart including the experimental steps is indicated in Fig.1.

FT-IR spectra were applied to determine the oxygen-including groups in the produced prepared nanomaterial. The thickness of the GONSs was specified by AFM. To determine the oxidation degree in the synthesized GONSs, a UV/vis spectroscopy measurement was used. The expansion of GO layers and dispersion of GONSs in the structure of GO/PAM nanocomposites were determined using XRD. The induced disorder degree during the oxidation process of graphite and the GONSs' number of layers was determined by Raman spectroscopy. Structural properties

and morphological of GONSs and synthesis of nanocomposites were characterized by FESEM. Thermal properties of the prepared nanomaterial were evaluated using Simultaneous Thermal Analysis (STA) that investigated both TGA and DTA. Thermal conductivity analyzer (Heat Conduction Unit) was used to measure the thermal conductivity of the synthesized nanomaterials. Rheological properties of the prepared nanomaterials were measured using an Anton Paar strain-controlled rheometer (MCR301).

EXPERIMENTAL SECTION

Materials

Natural flake graphite (90%), H_2SO_4 (>98%), H_3PO_4 (85%), $KMnO_4$ (>99%), H_2O_2 (>30%), HCl (37%), anhydrous ethanol, and anhydrous ethyl ether (99%) were purchased from Merck Chemical Company. Acrylamide (AM, >98%), ammonium peroxodisulfate (APS) were supplied by Fluka.

GONSs Preparation

GONSs were synthesized using a procedure in which graphite flake was oxidized by a mixture of H_2SO_4:H_3PO_4 (4:1) and $KMnO_4$. The graphite flake (3 g), H_2SO_4 (320 ml), and H_3PO_4 (80 ml) were increased to a 1 L round-bottom flask at room temperature. While the mixture was stirring, $KMnO_4$ (18 g) was gradually increased to flask contents and mixed for 72 h without temperature control. After 3 days, the dark purplish green-mixture color changed to dark brown, indicating the oxidation was completed and the reaction was stopped by increasing H_2O_2. After 24 h, the suspension of oxidized graphite was separated and washed with 1 M of HCl in three steps. The precipitate was re-suspended by shaking with deionized water (1 L in any time) into a 2 L beaker until a pH of 4-5 was achieved. Purifying and washing steps were performed via a centrifugation technique at 4500 rpm for an hour. After obtaining the desired pH, sedimentation and re-suspension were performed again with a mixture of anhydrous ethanol and water (2 : 1) and the product was finally washed with anhydrous ethyl ether and dried under vacuum at 50˚C for 4 h. The washing process not only purified the product but also exfoliated the graphene oxide [56].

GO/ PAM Nanocomposite Preparation

Solution polymerization in aqueous medium was employed to synthesize GO/PAM nanocomposites. Prior polymerization process, GONSs (0.5 wt. %) were suspended in deionized water (40 ml) by a powerful magnetic stirrer for 30 min. GONSs were completely dispersed in water by ultrasonic technique (140 watts, 20 kHz) for 30 min at 25˚C. Then, the dispersed GONSs were increased to the dissolved AM (20 g) in fresh water (80 ml) at ambient temperature. The suspension of the mixture was transferred into a three-neck round bottom flask in a water bath under a continuous flow of nitrogen. An electrical mixer and a condenser were provided for the reaction container. For the removal of dissolved oxygen of the mixture (before the beginning of polymerization), the nitrogen bubbling was used for 15 min. The polymerization was carried out by adding 5 cc APS (0.05 wt. % in water) to the reaction flask via a needle and increasing the bath temperature up to 67˚C and of 300 rpm (stirring rate) all over the reaction time. The polymerization was performed in 20 minutes and the obtained nanocomposites were cut into pieces, and the unreacted monomers were removed from the product via washing it three times by a mixture of ethanol and water (80:20 v/v). They were then spread on the smooth surface and dried at 65˚C. In order to synthesize other samples (pure PAM and GO/PAM nanocomposites with GONSs (1, 1.5, 2 wt. %)), the reaction was performed again. The schematic of this process is shown in Fig.2a.

Characterization

FT-IR spectra were used to determine the internal network structure of the synthesized nanomaterial by a Bruker Spectrometer in a range of 400-4000 cm^{-1}. XRD spectra were employed to measure the interlayer spacing of GONSs as well as exfoliation and dispersion of GONSs in the PAM matrix by a Bruker D8 with the scattering angles between 10˚ and 80˚ with the increase of 0.05˚. The determination of GONSs thickness was carried out by AFM (Agilent 5500) in a tapping mode. The definition of the oxidation level in the synthesized GONSs was performed by UV/vis spectroscopy. Raman spectrum of GONSs was obtained using microspectrometer (Takram P50C0R10) at the laser wavenumber of 532 nm, between 1000 and 3500 cm^{-1}. The determination of thermal stability of the synthesized nanomaterial was obtained by STA (B-HR) that investigated both TGA and DTA from ambient temperature up 700˚C and 10˚C/ min. FESEM (MIRA 3 Tescan-XMU) was utilized

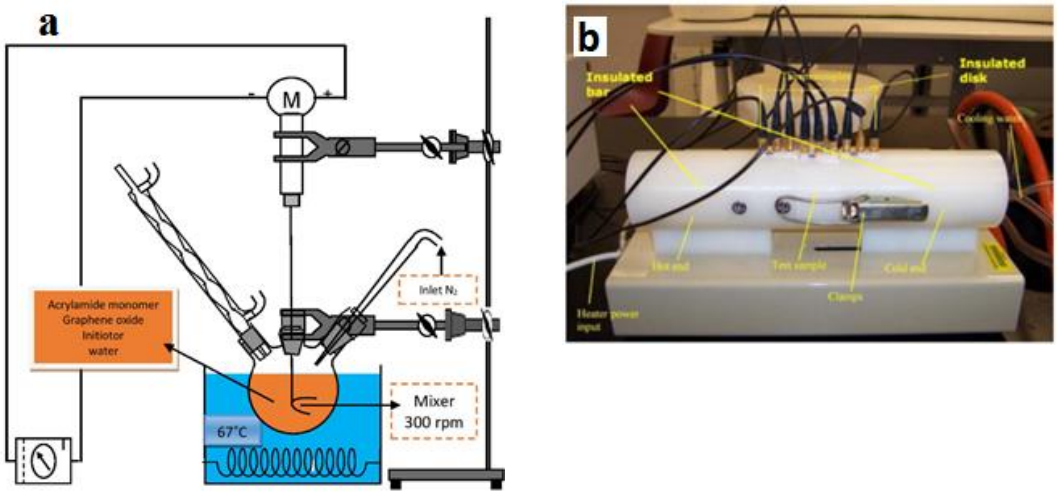

Fig. 2. A schematic of GO/PAM nanocomposites synthesis process (a), and (b) a photograph of Heat Conduction Unit.

to determine the morphology of the synthesized nanomaterial.

Rheological measurements of the prepared nanomaterials were performed by Anton Paar strain-controlled Rheometer (MCR302). To determine the linear viscoelastic properties, storage, and loss modulus were evaluated at a constant strain of 0.1%. The frequency sweep was performed from ω =0.1 to 100 rad/s on each synthesized nanomaterial. To investigate the viscoelastic properties of GONSs, the hydrogel which was prepared by mixing a certain volume GONSs with the solution of hydrochloride acid with pH=0.6 was used [57]. The powdered form of PAM and GO/PAM nanocomposites was poured on the measuring plate of a device for studying their viscoelastic properties. The evaluations were performed at 25 ˚C.

Thermal conductivity analyzer (heat conduction unit, H940) was used to measure the thermal conductivity of the synthesized nanocomposites and PAM. The heat conduction unit is presented in Fig. 2b. The unit is isolated and its temperature is controlled by several thermocouples at specified locations. As can be seen in Fig. 2b, the unit contains a hot end which was supplied from one of the brass terminals through a heater and a cold end which was cooled by circulating water at 400 ml/min in contact with the brass terminal and test samples. This system can determine the thermal conductivity of a sample by measuring the temperature difference between hot and cool sources and solving Eq.1 on the principle of Fourier's Law.

$$Q=-kA\frac{dT}{dx} \quad (1)$$

Where Q is the heat flow rate (W), k is the thermal conductivity constant ($W.m^{-1}.K^{-1}$), dT/dx is the temperature gradient ($K\cdot m^{-1}$), and A shows the area of the sample (dimension of samples was about 25 mm in diameter and 4 mm in thickness).

RESULTS AND DISCUSSION

Preparation and characterization of GO

Simplified Hummer's procedure was performed to synthesize GONSs. This method, unlike the generally practical technique that is involved in controlling the temperature during the process of graphite oxidation, such as keeping the temperature low during while $KMnO_4$ is increased as well as keeping the temperature high along the oxidation step, is not difficult and tedious. This procedure is relatively secure and the danger of outbursts has been extremely decreased. moreover, washing and purgation steps are easy and yield to a high transformation of GONSs [58]. The washing and purification process of GONSs, which was carried out by washing using fresh water, involves the lamination into single or a few layers GONSs. It can be said that the hydration of GONSs layers is performed by hydrogen bonding and the interactions between oxygen-containing groups of GONSs layers and water which affords

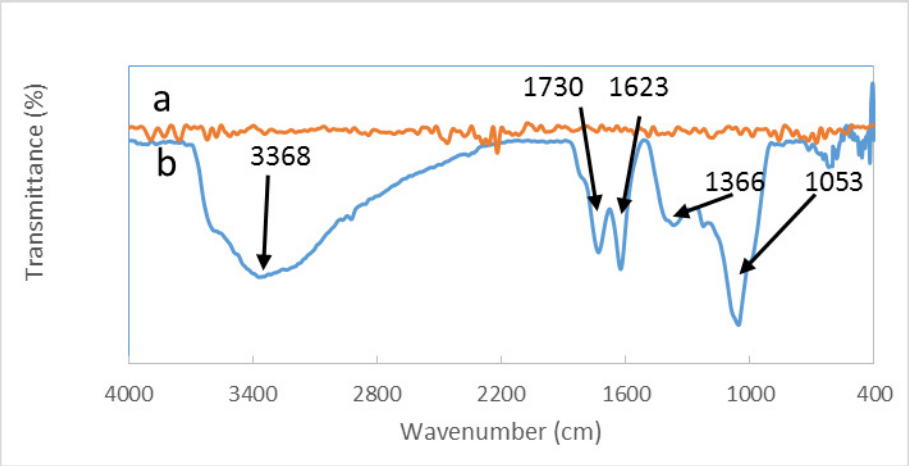

Fig. 3. FT-IR spectra of graphite flake (a), and synthesized GONSs (b).

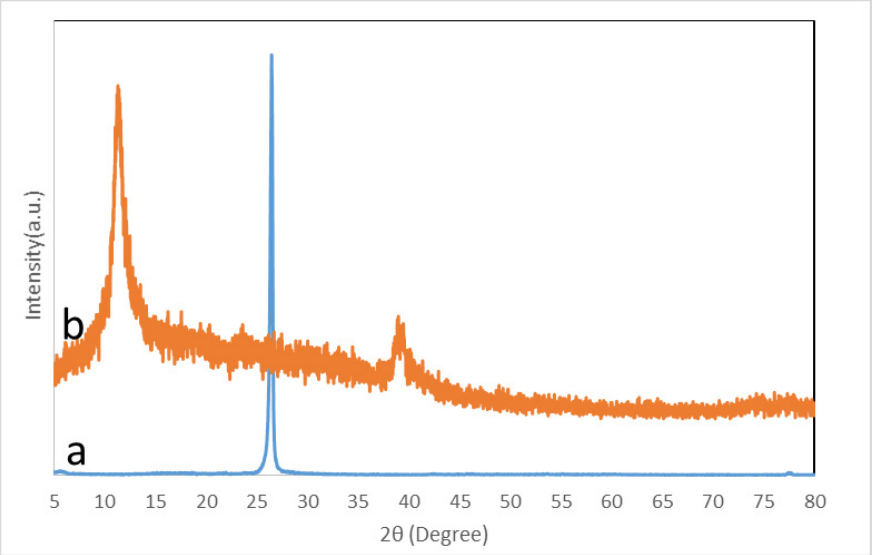

Fig. 4. XRD of graphite flake (a), and synthesized GONSs (b).

the exfoliation of GO layers [56].

FT-IR spectrum of the GONSs was used to analyze the oxygen-containing groups on the surface of GONSs. As can be seen in the spectrum pattern of graphite (Fig. 3a), there were no peaks in the resulted vibrations. Fig. 3b indicates the adsorption bands of GONSs at 1730 cm^{-1}, 1623 cm^{-1}, 1366 cm^{-1}, 1225 cm^{-1}, and a wide peak at 3368 cm^{-1} that are respectively related to C=O stretching vibration, vibration of unoxidized C=C bonds, C-OH stretching vibration, C-O-C stretching, and O-H stretching vibration. C-O stretching of carboxylic acid was observed at 1053 cm^{-1} [59, 60]. The existence of these adsorption bands (Fig. 3) confirmed the formation of oxygen-including groups on the surface of GONSs. Depending on the location and intensity of the absorption peaks of GONSs, it can be said that although epoxy and hydroxyl groups are grafted on both edges and surfaces, carboxyl groups are mostly connected on the edges of GONSs [61].

For evaluation of GONSs exfoliation and dispersion of GONSs in the synthesized nanocomposites structure, XRD was employed. The XRD spectra of graphite flake and GONSs are represented in Fig. 4. Based on this figure, a sharp

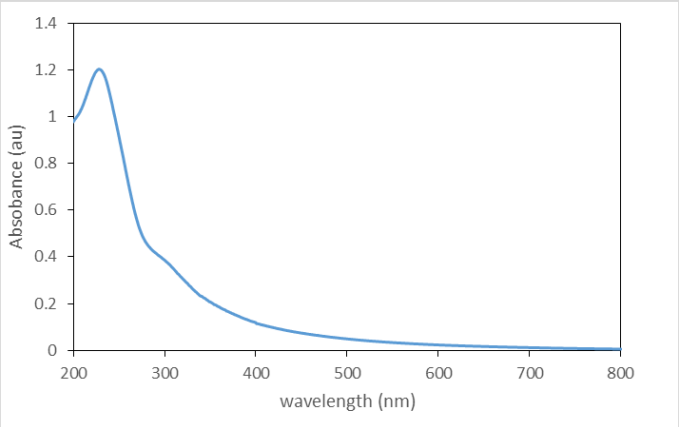

Fig. 5. UV/vis spectrum of synthesized GONSs.

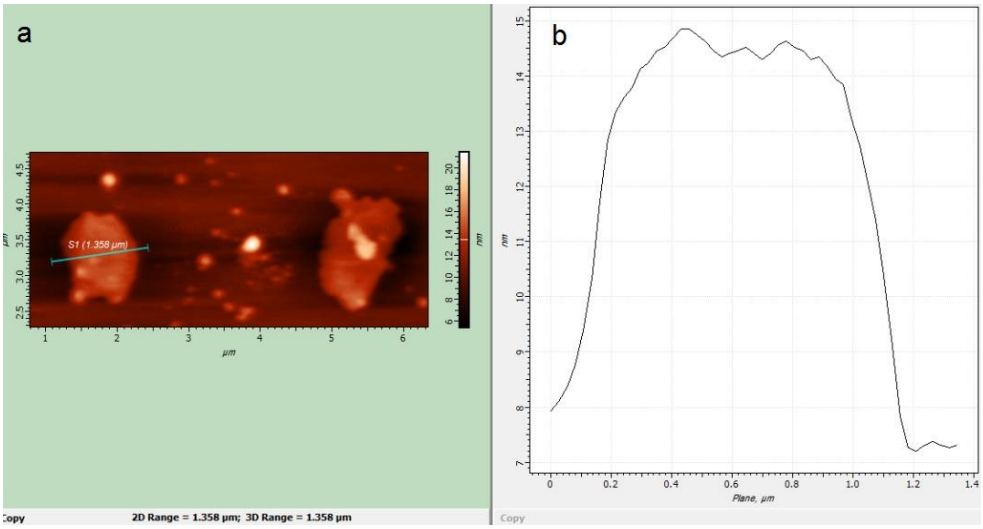

Fig. 6. AFM measurement of synthesized GONSs. AFM image (a), and height profiles of synthesized GONSs (b).

peak at 2θ = 26.48 is observed in the pattern of graphite XRD spectrum which is related to the entity of graphite flake (Fig. 4a) while the distance of layers was measured to be about 0.336 nm using Brag's Law. The lack of any remaining phase and the existence of a sharp peak in the XRD spectrum of graphite indicate that it has excellent purity. As can be seen in Fig. 4b, a peak is observed at 2θ = 11.32 which is associated with the existence of GONSs while the distance of layers was measured to be about 0.781 nm. Increasing layer distances of GONSs presented that the oxidation process of graphite has been exactly performed via the weakening of the interlayer van der walls instructions [58, 62].

UV/vis spectroscopy evaluation was performed to specify the oxidation level of GONSs. Fig. 5 demonstrates the UV/vis spectrum of the prepared GONSs with a peak at 228 nm. This peak is related to the π → π* transition (conjugation) for the C=C bonding [18]. The peak location of GONSs represented that it has a lower content of residual conjugation and higher energy for the electronic transition which resulted in a higher level of oxidation with more oxygen-containing groups on the surface of GONSs [58].

AFM image was employed to define the GONSs thickness and the number of layers. Fig. 6a, and b shows an AFM image and the height profile of GONSs which is obtained under tapping mode. According to the obtained results, the thickness of the prepared GONSs was around 6.85 nm.

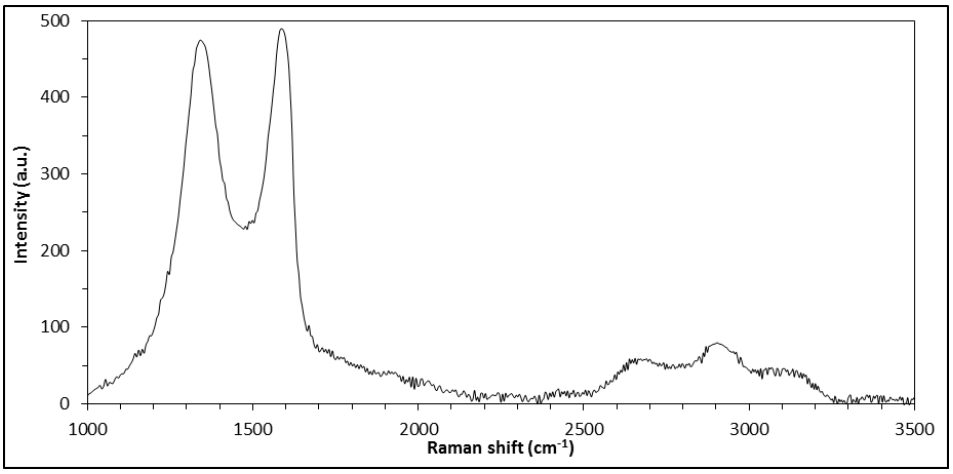

Fig. 7. Raman spectrum of synthesized GONSs.

It illustrates that the synthesized GONSs have few-layers. The AFM image (Fig 2a) presents the uniform sheets of synthesized GONSs with a dimension range of 1.358 μm.

Raman spectroscopy is employed to evaluate the nature of defects and the extent of chemical modification, as well as distinguishing single or multilayer graphene [63, 64]. The Raman spectrum of the synthesized GONSs (Fig. 7) exhibited three main characteristic peaks: 1) The peak at 1585 cm^{-1} (G band) which is related to phonon mode (E_{2g} symmetry) and originated from in-plane vibration of sp^2 carbon atom in a 2D hexagonal lattice. 2) The peak at 1350 cm^{-1} (D band) which is corresponded to the breathing mode of j-point phonons (A_{1g} symmetry) and arisen from the double resonance of induced disorder in graphite structure. 3) The peak at 2900 cm^{-1} which is related to the symmetry-allowed 2D overtone mode. Raman spectrum pattern of synthesized GONSs is in accordance with the reported spectrum for graphene oxide by Claramunt *et al.* and Lopez-Díaz *et al*. [65, 66]. Ferreira *et al.* showed that the 2D band intensity reduces when the disorder degree of graphene increases and it is replaced by a bulge [67]. The Raman spectrum of synthesized GONSs is completely in accordance with these findings.

Generally, the shape of the 2D band is related to the number of graphene layers and utilized to determine the number of its layers [68]. The 2D band for a single layer of graphene was interpreted as a single peak with a full width at half maximum (fwhm) of about 30 cm^{-1} [69]. By increasing the number of GONSs layers to two, three layers, or few-layers, the 2D band is decomposed into a wider and asymmetric peak [66]. As can be seen in Fig. 7, the 2D band was not a single peak. Based on these reasons, it can be concluded that the number of stacked layers of GONSs is few-layers.

The surface morphology of the graphite and GONSs was investigated by FESEM. As can be seen in Fig. 8a, the graphite flake is flat and has very sharp sides. Moreover, layers of graphite are closely attached to each other. Fig. 8b shows that the GONSs layers are extensively expanded. The process of oxidation included many oxygen-containing groups which formed a great number of disordered wrinkles and shrinkage on the surface of synthesized GONSs. The FESEM image of the GONSs indicated clear variations, particularly the smother edges of GONSs compared with the graphite.

Preparation and characterization of Go/PAM nanocomposites

GO/PAM nanocomposites synthesis was performed by in-situ polymerization in an aqueous medium. In a glass reactor, a definite amount of AM monomer was dissolved in deionized water and GONSs which were suspended in water via cell ultrasonic and mixed using a mechanical stirrer. The polymerization process and synthesis of GO/PAM nanocomposite were performed using the APS as an initiator and at a constant temperature of 67˚C. Steps of nanocomposites synthesis are schematically presented in Fig. 9. The GONSs have a high dispersion in aqueous due to the plentiful oxygen functional groups that are found

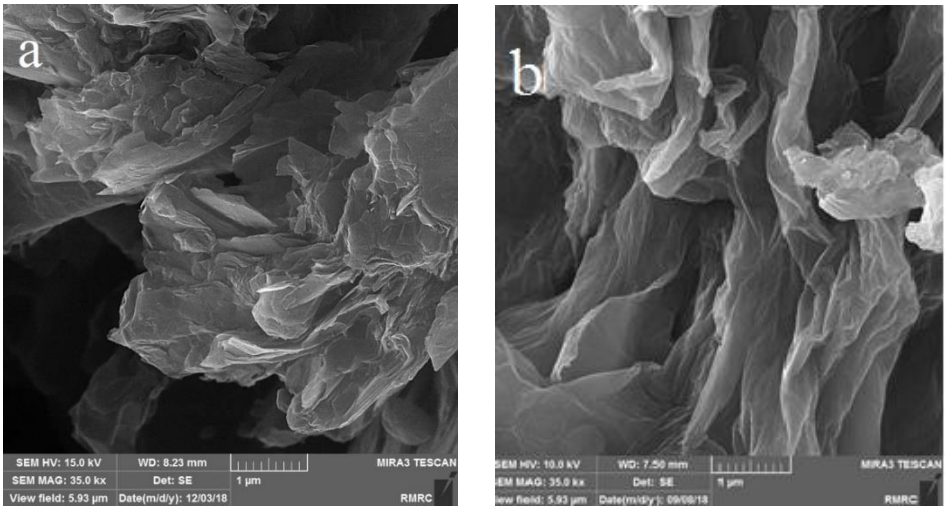

Fig. 8. FESEM images of graphite flake (a) and synthesized GONSs (b).

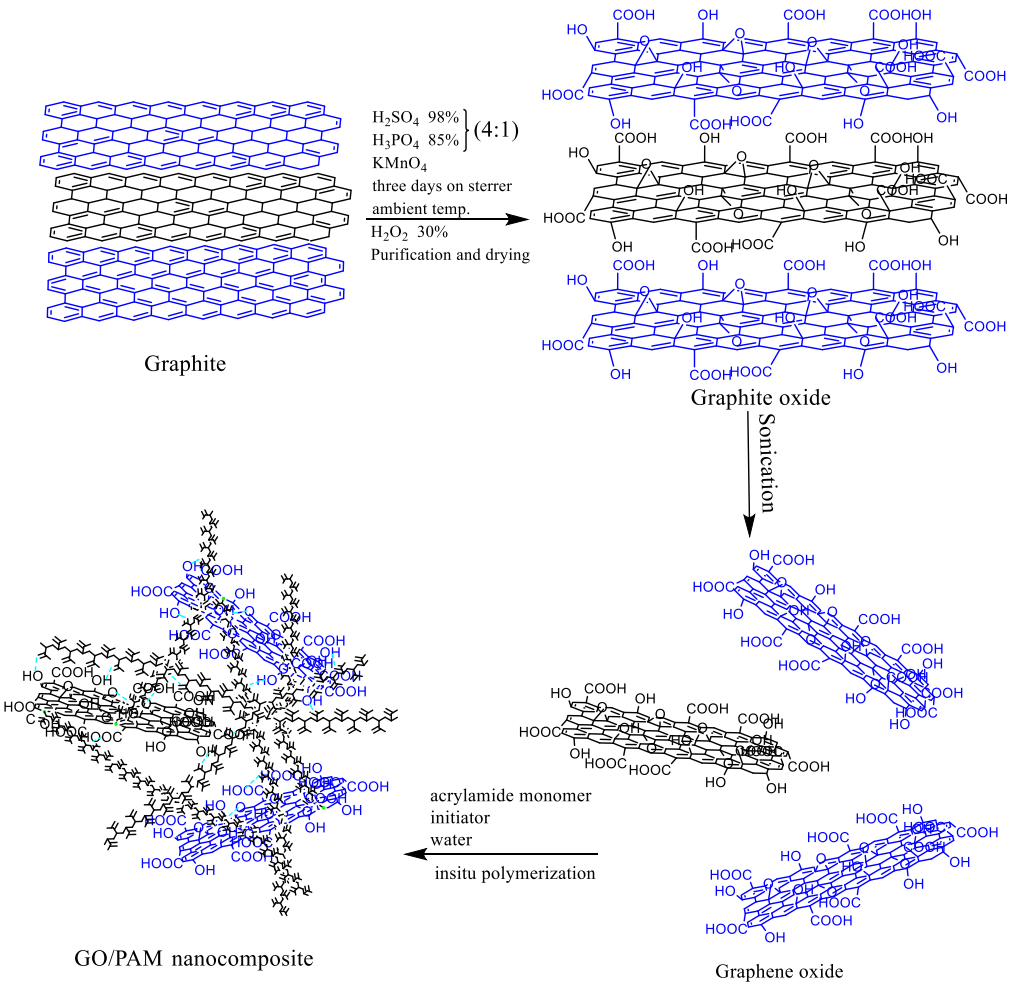

Fig. 9. A schematic of synthesis steps of nanocomposites.

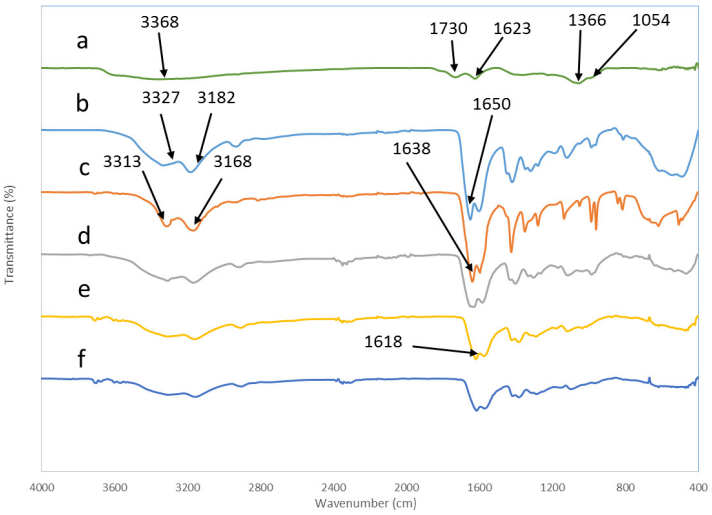

Fig. 10. FTIR spectrum of GONSs (a), pure PAM (b), $GO_{0.5}$/PAM nanocomposite (c), $GO_{1.0}$/PAM nanocomposite (d), $GO_{1.5}$/PAM nanocomposite (e), and $GO_{2.0}$/PAM nanocomposite (f).

on GONSs surfaces. On the other hand, there is an instruction between GONSs and PAM networks via the formation of bonding between oxygen-containing groups of GONSs and N-H or C=O bonds of PAM that resulted in the formation of a strong and interconnected network.

Verification of the chemical structures and successful preparation of PAM and GO/PAM nanocomposites were performed using FT-IR spectroscopy. Fig. 10 shows the FT-IR spectra of synthesized nanomaterial. By comparing the spectrum of GONSs (Fig. 10a) and other spectra, it was observed that intensive peaks of GONSs were not revealed in PAM and nanocomposites spectra that illustrated GONSs were tightly inscribed by PAM chains. In Fig. 10b, stretching vibration of N-H are seen at absorption peaks of 3327, and 3182 cm^{-1}. The wavelengths of 1602 and 1650 cm^{-1} are also attributed to N-H deformation and C=O stretching vibration. Special absorption bands at 1419 and 1120 cm^{-1} are respectively corresponded to CH_2 and NH_2 in-plane vibration and rocking of PAM. By adding GONSs (0.5 wt. %) to PAM structure, N-H absorption peaks of $GO_{0.5}$/PAM nanocomposite (3313, and 3168 cm^{-1}) shifted to smaller wavelengths (Fig 10c). Moreover, a powerful peak at 1638 cm^{-1} is attributed to the C=O vibration of the amide groups. Shifting in a location of absorption peaks is due to the creation of a bond between oxygen-activated groups on the surface and edges of GONSs and amide or carbonyl of PAM [70]. Shifting absorption peaks to smaller wavelengths is also observed in the other GO/PAM nanocomposites (Fig. 10 d-f) in comparison to the PAM which caused an increment in hydrogen bonding formation.

In order to have more investigation in the synthesis of GO/PAM nanocomposites and the dispersion degree of GONSs in nanocomposite structure, the XRD technique was carried out. This is an important technique for determining the existence or the absence of GONSs aggregation in the polymer matrix [71]. Fig. 11 demonstrates the XRD of synthesized nanomaterial. It is clear that the vigorous peak of GONSs at 11.3° (Fig 11a) is not revealed in all of the XRD curves of nanocomposites which illustrates that GONSs were sorely dispersed in the matrix [72]. In the XRD patterns of the synthesized PAM and GO/PAM nanocomposites (Fig. 11b-e), a broad peak from 6° to 32° is observed which is related to the scattering of PAM and their formless nature. Furthermore, the XRD curves of the synthesized nanocomposites indicated that there were no clear changes at the profile of diffraction peaks compared to that of PAM, implying that the GO/PAM nanocomposites had the same amorphous feature as that cross-linked PAM. Actually, the suitable distribution of GONSs in the PAM does not imply their good dispersion and interface in the composites which will be confirmed in the FESEM images [72].

FESEM images (Fig. 12) provide morphological

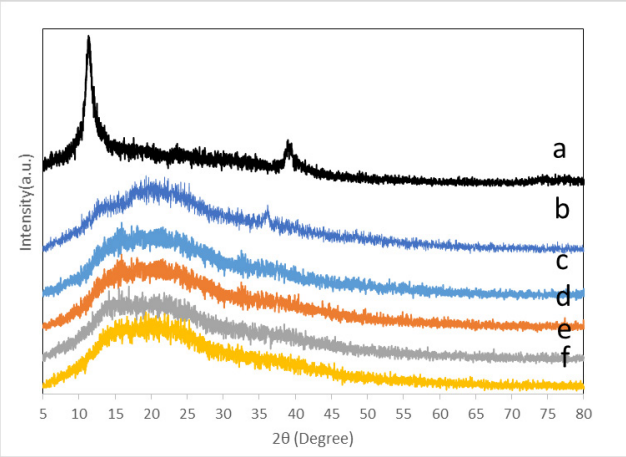

Fig. 11. XRD of GONSs (a), pure PAM (b), $GO_{0.5}$/PAM nanocomposite (c), $GO_{1.0}$/PAM nanocomposite (d), $GO_{1.5}$/PAM nanocomposite (e), and $GO_{2.0}$/PAM nanocomposite (f).

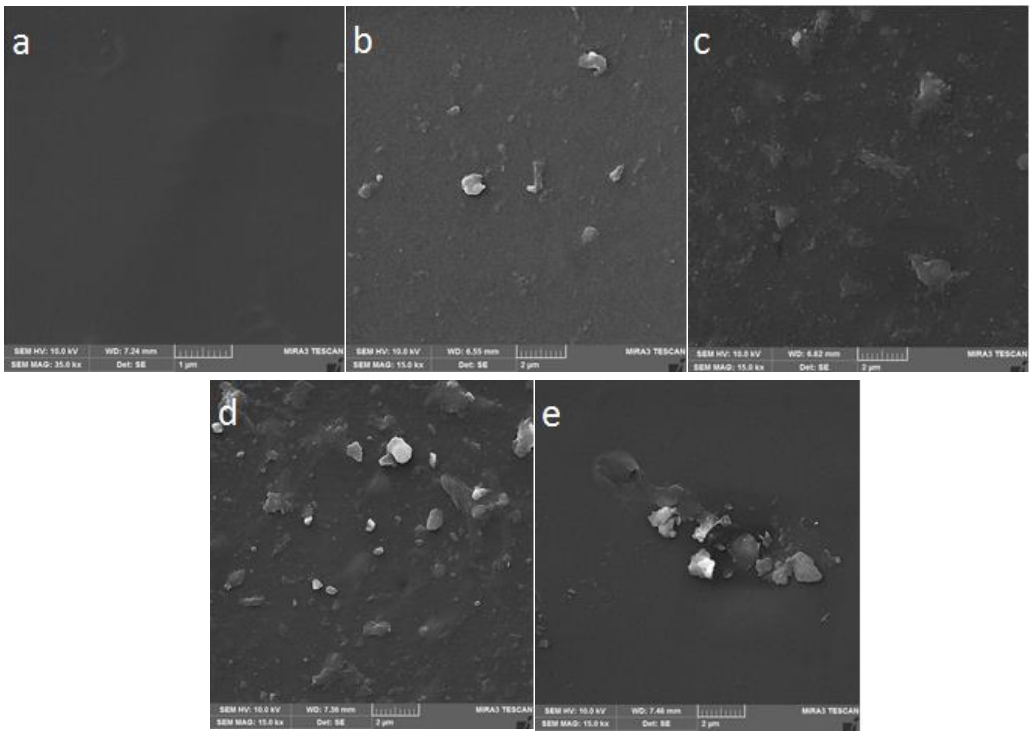

Fig. 12. FESEM images of surface of pure PAM (a), $GO_{0.5}$/PAM nanocomposite (b), $GO_{1.0}$/PAM nanocomposite (c), $GO_{1.5}$/PAM nanocomposite (d), and $GO_{2.0}$/PAM nanocomposite (e).

information of the synthesized PAM and nanocomposites and confirm their successful fabrication. Fig. 12a indicates the relatively compact and smooth surface of pure PAM. It can be due to the interconnection of PAM chains [50]. Figs. 12b-d shows the FESEM picture of homogeneous nanocomposites. As it can be seen, the surfaces compactness is increased that can be related to the affirmative influence of GONSs in the enhancement of PAM chain interactions and improvement of network strength. By increasing GONSs content (Fig. 12e), the surface density of the synthesized $GO_{2.0}$/PAM nanocomposite is decreased in comparison to other synthesized

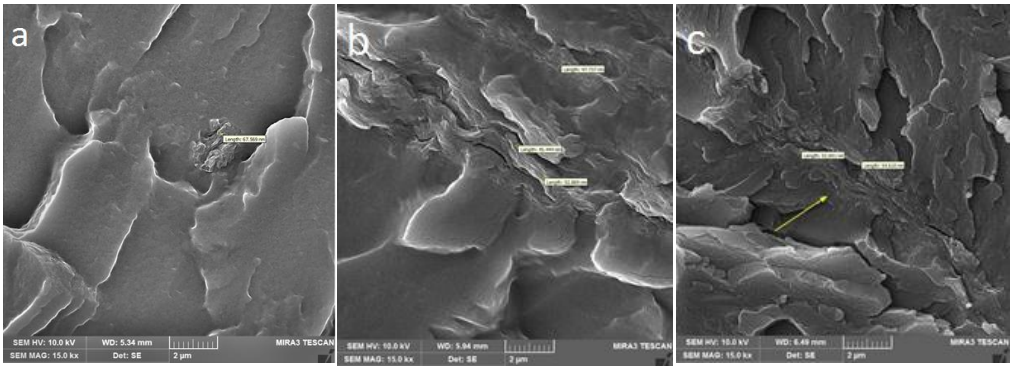

Fig. 13. FESEM images of fractured surfaces of $GO_{1.0}$/PAM nanocomposite (a), $GO_{1.5}$/PAM nanocomposite (b), and $GO_{2.0}$/PAM nanocomposite (c).

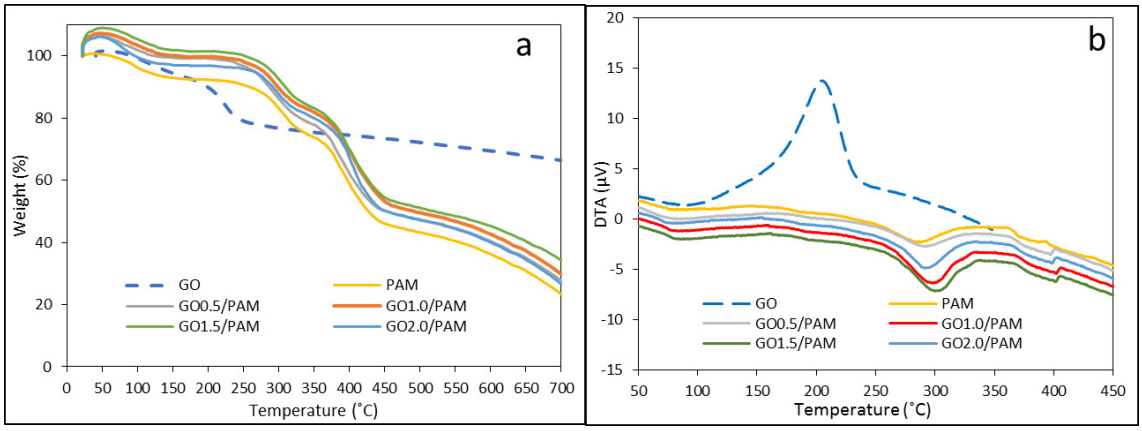

Fig. 14. TGA (a) and DTA (b) diagram of synthesized samples.

nanocomposites which is appeared because of the agglomeration of a dispersed phase in the polymer matrix. Fig. 13a-c confirms the presence of GONSs in the fractured surface structure of nanocomposites. Generally, it can be said that the GONSs are firmly embedded into the PAM chains demonstrating fine adaptability and powerful interconnection between GONSs and PAM [73].

Fig. 14 shows the DTA and TGA curves which were employed to characterize the thermal properties of the synthesized nanocomposites in comparison to the polymer base. Mass losing of GONSs was begun at below 100˚C and 15% of the weight was approximately lost at around 250˚C. It can be attributed to the thermal degradation of the unstable oxygen-activated groups that were converted to carbon monoxide, carbon dioxide, and steam [74]. Mass losing from 250 to 700 °C became slower than lower temperatures that can be related to the elimination of more stable oxygen-containing groups [75]. Weight losing of the synthesized GONSs is totally around 34% at 700 °C. As can be seen, the addition of GONSs as filler to PAM as a matrix has improved the thermal stability of GO/PAM nanocomposites while the most stable thermally of the synthesized nanocomposites occurred in 1.5 % of GONSs content. Fig. 14a shows a similar trend of the synthesized nanocomposites at TGA and two main points of weight loss that yielded to the degradation of oxygen-activated groups and carbonization of PAM [76]. The maximum residual content was observed in the synthesized nanocomposite with 1.5 wt. % of GONSs content which was about 34.25% at 700 °C compared with pure PAM (23.3%). Decomposition point and residual content enhancement are related to mobility limitation of GO/PAM nanocomposites which is resulted from powerful instructions that are created due to the presence of GONSs in nanocomposites [49]. The

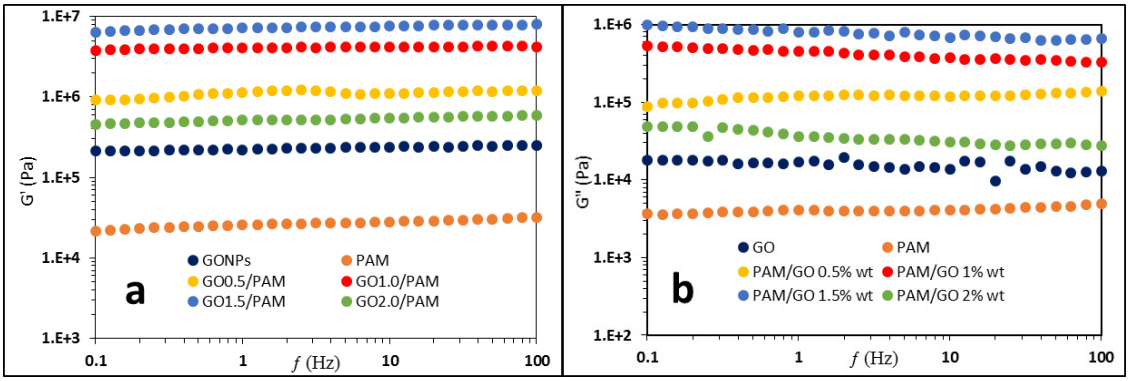

Fig. 15. Oscillation frequency scanning: The elastic modulus (G') (a), and the viscous modulus (G") (b) of synthesized samples.

thermal properties and residual content of $GO_{2.0}$/PAM nanocomposite were reduced compared with $GO_{1.5}$/PAM nanocomposite which can be due to the aggregation of GONSs in nanocomposite network and the evidences of agglomeration that are observed in its FESEM image. Fig. 14b shows the glass transition temperature (Tg) of the synthesized samples. As it is clear, Tg of $GO_{1.5}$/PAM nanocomposites (74.6 °C) are enhanced compared with pure PAM (83 °C). This result can be related to the formation of bonding because of the internal interaction between the oxygen-activated groups and amide or carbonyl of GONSs and PAM, respectively [77]. Improvement of Tg and enhancement of melting point from PAM (283.9˚C) to $GO_{1.5}$/PAM nanocomposites (299.8˚C) illustrated that the addition of GONSs content led to an increment in nanocomposites crystallinity and improvement in the thermal properties in comparison to the PAM [78].

The improvement trend of the thermal properties of synthesized nanocomposites was similar to the most recent studies. Alpaslan *et al.* showed that the addition of Citric Acid (CA) Red Apple peel Extract (RApE) to the hydrogel (N, N dimethyl acrylamide (DMAAm)-co-gelatin) improved the thermal stabilities of the synthesized hydrogels [79]. The results of Patole *et al*. research demonstrated that the addition of graphene at different amounts to polystyrene enhanced the thermal properties and increased T_g of synthesized nanocomposites [80].

Rheology is the science that investigates the behavior of deformation and flow of all kinds of material [81]. Rheological property of polymer nanocomposites provides a deep understanding of the internal structure of these materials which can be investigated by evaluating viscoelasticity. Oscillation frequency was used to specify the viscoelasticity of the synthesized GO/PAM nanocomposites. Fig. 15 shows the storage modulus (G') and loss modulus (G") with frequency for GO, PAM, and GO/PAM nanocomposites. G' is attributed with the capability of the material to the storage (stored) energy that is the elastic response and G" is associated with the capability to the lose (loss) energy that is the vicious response when an oscillatory force is applied [82]. Actually, G' demonstrates elastic portion and G" indicates the viscous portion of viscoelastic behavior. As can be seen in Fig. 15, G' is much higher than G" in the investigated frequency region implying that elastic property is higher. Fig. 15a, b shows that at the constant concentration of PAM and different GONSs content (0.5, 1, 1.5, and 2 wt. %), the values of G' and G" of nanocomposites are increased in comparison to the PAM. For example, in PAM, G' and G" values were respectively about 21.6 KPa and 3.63 KPa while loading GONSs (0.5 wt. %) to PAM led to a remarkable increment in values of G' and G" to 909 KPa and 88.5 KPa respectively, implying synergistic effect of the GONSs. Also, this significant increase shows that the GONSs has good dispersion in the polymer structure[48]. Increasing trend of G' and G" continued in other nanocomposites with GONSs content (1 and 1.5 wt. %), while in nanocomposite with 2 wt. % of GONSs content was inverted (G' and G" was 456 KPa and 48.4 KPa, respectively). These results confirmed that agglomeration in $GO_{2.0}$/PAM is partly occurred. The remarkable enhancement in G' and G" with the loading of GONSs in PAM represents that there are strong instructions between the GONSs and PAM chains.

These instructions compact the network structure of PAM and increase the G' and G" of synthesized nanocomposites.

Comparing rheological properties of synthesized nanocomposites in this study with the results of recent researches showed a remarkable improvement [83, 84]. Yang *et al.* showed that G' and G" of hydrogel composite (graphene oxide/ polyacrylamide) at the constant concentration of polyacrylamide (2 mg ml^{-1}) and graphene oxide (5 mg ml^{-1}) improved to about 15000 and 1130 Pa, respectively [84]. The increase of G' and G" in their study was obtained by a high value of graphene oxide while in our research was used a very little value of it.

As previously mentioned, the basis for the calculation of the thermal conductivity is the liner conduction in the axial direction and the use of Fourier's law. Since the temperature gradient is measured in an axial direction, it is necessary to transfer and measure the heat flux in the axial direction. For this purpose, the hot end, cool end, and sample place are isolated in a radial direction. It should be noted that the synthesized nanocomposite has a low thermal conductivity and as a result, the heat transferred in the radial direction cannot be ignored compared with the axial direction. Therefore, two values of heat flux are used to calculate the thermal conductivity, and the average of the measured thermal conductivities was reported as the thermal conductivity. Table 1 shows the thermal conductivity of the synthesized nanocomposites and pure PAM. As can be seen in Table 1, the synthesized nanocomposites have greater values of thermal conductivity than that of PAM which illustrated the outstanding effect of GONSs on thermal conductivity of nanocomposites. $GO_{0.5}$/PAM nanocomposite showed 0.68 $W.m^{-1}.K^{-1}$ which increased about 39% compared to pure PAM with 0.49 $W.m^{-1}.K^{-1}$ in thermal conductivity (Table 1). Increasing the thermal conductivity of nanocomposites with GONSs as a filler is related to the interfacial instruction between the polymer and GONSs [85]. The oxygen-activated groups on the surface of GONSs can react with N-H and C□O of PAM in formation of the in-situ polymerization, which connect the PAM chain with GONSs by hydrogen bonding. Notably, these bondings have increased interfacial interactions and decrease interfacial thermal resistance. Fig. d9 shows the schematic of the interfacial interaction between the GONSs and the PAM chains. The

Table. 1. Thermal conductivity of pure PAM, and GO/PAM nanocomposites.

Sample	Thermal conductivity, $W.\ m^{-1}.\ K^{-1}$
PAM	0.49
$GO_{0.5}$/PAM	0.68
$GO_{1.0}$/PAM	0.81
$GO_{1.5}$/PAM	0.90
$GO_{2.0}$/PAM	0.74

nanocomposite with 1.5 wt. % of GONSs content increased the thermal conductivity to 0.9 $W.m^{-1}.K^{-1}$ while $GO_{2.0}$/PAM nanocomposite decreased the thermal conductivity to 0.74 $W.\ m^{-1}.\ K^{-1}$. This variation of trend is attributed to the occurrence of the agglomeration of GONSs in the structure of the synthesized nanocomposite while interfacial instruction between PAM and GONSs was decreased.

The resultant thermal conductivity of PAM and synthesized nanocomposites in this study comparing with Tseng *et al.* research showed the same trend [86]. They studied the effect of addition graphene oxide (GO) and glycidyl methacrylate-grafted graphene oxide (g-GO) in the Polyimide (PU). They found that the thermal conductivity of GO /PU nanocomposites was increased by addition of GO from 0.3 to 10 wt. % [86]. It is clear that the added amounts of GO in our study are much less.

CONCLUSION

Solution polymerization in aqueous medium was employed to synthesize the polymer nanocomposites in which PAM as a base phase and GONSs as a filler were used to fabricate the GO/PAM nanocomposite with different GONSs content (0.5, 1, 1.5, and 2 wt. %). Improved Hummer's method was used to synthesize the required GONSs which, unlike other general technique, is hassle-free. The internal chemical structure of the synthesized nanomaterial was evaluated by XRD, FT-IR, FESEM, TGA, and DTA. AFM was used to evaluate the thickness of GONSs. The oxidation level of GONSs was determined by UV/vis spectroscopy measurement. The Raman spectrum of the synthesized GONSs showed three peaks at 1350, 1585, and 2900 that are related to the D, G, and 2D bands. Evaluation of Raman spectroscopy of GONSs represented that the disorder degree of graphene was increased while the number of GONSs layers was few-layers. The result showed that the fine compatibility between PAM and GONSs was created in a synthesized

nanocomposite structure that not only made the structure stronger and more interconnected, but also significantly improved rheological properties and thermal conductivity compared with the pure PAM. These results were confirmed by the obtained evidences from FESEM images and thermal property analyses. This research provides a convenient and fast way to synthesize inorganic/organic nanocomposites with superior elastic properties by solution polymerization in aqueous disperse systems. The significant improvement of viscoelastic behavior and thermal conductivity suggest the potential application of GO/PAM nanocomposite in the field of water-based drilling fluid for enhancing the rheology and thermal conductivity properties of drilling mud.

CONFLICT OF INTEREST

The authors declare that they have no competing interests.

REFERENCES

1. Balandin A. A., Ghosh S., Bao W., Calizo I., Teweldebrhan D., Miao F., Lau C. N., (2008), Superior thermal conductivity of single-layer Graphene. *Nano Lett.* 8: 902-907.
2. Castro Neto A. H., Guinea F., Peres N. M. R., Novoselov K. S., Geim A. K., (2009), The electronic properties of graphene. *Rev. Modern Phys.* 81: 109-162.
3. Lee C., Wei X., Kysar J. W., Hone J., (2008), Measurement of the elastic properties and intrinsic strength of monolayer graphene. *Science*. 321: 385-388.
4. Novoselov K. S., Geim A. K., Morozov S. V., Jiang D., Zhang Y., Dubonos S. V., Firsov A. A., (2004), Electric field effect in atomically thin carbon films. *Science*. 306: 666-669.
5. Geim A. K., Novoselov K. S., (2007), The rise of graphene. *Nat. Mater.* 6: 183-191.
6. Rafiee M. A., Rafiee J., Wang Z., Song H., Yu Z. Z., Koratkar N., (2009), Enhanced mechanical properties of nanocomposites at low graphene content. *ACS Nano*. 3: 3884-3890.
7. Tai Z., Yang J., Qi Y., Yan X., Xue Q., (2013), Synthesis of a graphene oxide–polyacrylic acid nanocomposite hydrogel and its swelling and electroresponsive properties. *RSC Adv.* 3: 12751-12757.
8. Fan J., Shi Z., Lian M., Li H., Yin J., (2013), Mechanically strong graphene oxide/sodium alginate/polyacrylamide nanocomposite hydrogel with improved dye adsorption capacity. *J. Mater. Chem. A.* 1: 7433-7443.
9. Stoller M. D., Park S., Zhu Y., An J., Ruoff R. S., (2008), Graphene-Based ultracapacitors. *Nano Lett.* 8: 3498-3502.
10. Xu Z., Gao C., (2010), In situ polymerization approach to graphene-reinforced nylon-6 composites. *Macromolecules*. 43: 6716-6723.
11. Lei Y., Chen F., Luo Y., Zhang L., (2014), Synthesis of three-dimensional graphene oxide foam for the removal of heavy metal ions. *Chem. Phys. Lett.* 593: 122-127.
12. Paredes J. I., Villar-Rodil S., Martínez-Alonso A., Tascón J. M. D., (2008), Graphene Oxide dispersions in organic solvents. *Langmuir*. 24: 10560-10564.
13. Li M.-j., Liu C.-m., Xie Y.-b., Cao H.-b., Zhao H., Zhang Y., (2014), The evolution of surface charge on graphene oxide during the reduction and its application in electroanalysis. Carbon. 66: 302-311.
14. Zhang M., Li Y., Su Z., Wei G., (2015), Recent advances in the synthesis and applications of graphene–polymer nanocomposites. *Polym. Chem.* 6: 6107-6124.
15. Brodie B. C., (1859), XIII. On the atomic weight of graphite. *Philosophical Transactions of the Royal Society of London*. 149: 249-259.
16. Staudenmaier L., (1898), Verfahren zur darstellung der graphitsäure. *Berichte Der Deutschen Chemischen Gesellschaft.* 31: 1481-1487.
17. Hummers W. S., Offeman R. E., (1958), Preparation of graphitic oxide. *J. Am. Chem. Soc.* 80: 1339-1339.
18. Marcano D. C., Kosynkin D. V., Berlin J. M., Sinitskii A., Sun Z., Slesarev A., Tour J. M., (2010), Improved synthesis of graphene oxide. *ACS Nano*. 4: 4806-4814.
19. Shen J., Hu Y., Shi M., Lu X., Qin C., Li C., Ye M., (2009), Fast and facile preparation of graphene oxide and reduced graphene oxide nanoplatelets. *Chem. Mater.* 21: 3514-3520.
20. Cai M., Thorpe D., Adamson D. H., Schniepp H. C., (2012), Methods of graphite exfoliation. *J. Mater. Chem.* 22: 24992-25002.
21. Berki P., László K., Tung N. T., Karger-Kocsis J., (2017), Natural rubber/graphene oxide nanocomposites via melt and latex compounding: Comparison at very low graphene oxide content. *J. Reinf. Plast. Compos.* 36: 808-817.
22. Santana G. J., Ortiz A., Oliveira R., Rangari V., Güven O., Moura E., (2017), Mechanical, thermal, morphology and barrier properties of flexible film based on polyethylene-ethylene vinyl alcohol blend reinforced with graphene oxide. *Characteriz. Mine. Metals, Mater.* (BOOK. pp: 49-57).
23. Kim H., Miura Y., Macosko C. W., (2010), Graphene/polyurethane nanocomposites for improved gas barrier and electrical conductivity. *Chem. Mater.* 22: 3441-3450.
24. Kim H., Macosko C. W., (2008), Morphology and properties of polyester/exfoliated graphite nanocomposites. *Macromolecul.* 41: 3317-3327.
25. Heo S., Cho S. Y., Kim D. H., Choi Y., Park H. H., Jin H.-J., (2012), Improved thermal properties of graphene oxide-incorporated Poly(methyl methacrylate) microspheres. *J. Nanosc. Nanotechnol.* 12: 5990-5994.
26. Wang Y., Liao X., Li S., Luo Y., Yang Q., Li G., (2016), Poly(methyl methacrylate) nanocomposites based on graphene oxide: A comparative investigation of the effects of surface chemistry on properties and foaming behavior. *Polym. Int.* 65: 1195-1203.
27. Baruah P., Karak N., (2016), Bio-based tough hyperbranched epoxy/graphene oxide nanocomposite with enhanced biodegradability attribute. *Polym. Degrad. Stab.* 129: 26-33.
28. Feng L., Guan G., Li C., Zhang D., Xiao Y., Zheng L., Zhu W., (2013), In situ synthesis of poly(methyl methacrylate)/graphene oxide nanocomposites using thermal-initiated and graphene oxide-initiated polymerization. *J. Macromol. Sci. Part A.* 50: 720-727.
29. Ma L., Wang G., Dai J., (2016), Preparation and properties of graphene oxide/polyimide composites by in situ

polymerization and thermal imidization process. *High Perf. Polym.* 29: 187-196.
30. Lu Y., Hao J., Xiao G., Zhao H., Hu Z., Wang T., (2017), In situ polymerization and performance of alicyclic polyimide/ graphene oxide nanocomposites derived from 6FAPB and CBDA. *Appl. Surf. Sci.* 394: 78-86.
31. Pan C., Liu L., Chen Q., Zhang Q., Guo G., (2017), Tough, stretchable, compressive novel polymer/graphene oxide nanocomposite hydrogels with excellent self-healing performance. *ACS Appl. Mater. Interfac.* 9: 38052-38061.
32. Song X., Yang Y., Liu J., Zhao H., (2011), PS colloidal particles stabilized by graphene oxide. *Langmuir*. 27: 1186-1191.
33. Gudarzi M. M., Sharif F., (2011), Self assembly of graphene oxide at the liquid–liquid interface: A new route to the fabrication of graphene based composites. *Soft Matter*. 7: 3432-3440.
34. Thickett S. C., Zetterlund P. B., (2013), Preparation of composite materials by using graphene oxide as a surfactant in Ab initio emulsion polymerization systems. *ACS Macro Lett.* 2: 630-634.
35. Ren L., Huang S., Zhang C., Wang R., Tjiu W. W., Liu T., (2012), Functionalization of graphene and grafting of temperature-responsive surfaces from graphene by ATRP "on water". *J. Nanopart. Res.* 14: 940-947.
36. Gonçalves G., Marques P. A. A. P., Barros-Timmons A., Bdkin I., Singh M. K., Emami N., Grácio J., (2010), Graphene oxide modified with PMMA via ATRP as a reinforcement filler. *J. Mater. Chem.* 20: 9927-9934.
37. Guo C., Zhao X., Zhang W., Bai H., Qin W., Song H., Qian X., (2017), Preparation of polymer brushes grafted graphene oxide by atom transfer radical polymerization as a new support for trypsin immobilization and efficient proteome digestion. *Anal. Bioanal. Chem.* 409: 4741-4749.
38. Nikdel M., Salami-Kalajahi M., Hosseini M. S., (2014), Synthesis of poly (2-hydroxyethyl methacrylate-co-acrylic acid)-grafted graphene oxide nanosheets via reversible addition–fragmentation chain transfer polymerization. *RSC Adv.* 4: 16743-16750.
39. Huynh V. T., Nguyen D., Such C. H., Hawkett B. S., (2015), Polymer coating of graphene oxide via reversible addition–fragmentation chain transfer mediated emulsion polymerization. *J. Polym. Sci. Part A: Polym. Chem.* 53: 1413-1421.
40. Khezri K., Najafi M., Roghani-Mamaqani H., (2017), Reversible addition fragmentation chain transfer polymerization of styrene from the edge of graphene oxide nanolayers. *J. Polym. Res.* 24: 34-39.
41. Gigmes D., Bertin D. , Lefay C., Guillaneuf Y., (2009), Kinetic modeling of nitroxide-mediated polymerization: Conditions for living and controlled polymerization. *Macromol. Theory Simul.* 18: 402-419.
42. García-Valdez O., Ledezma-Rodríguez R., Torres-Lubian R., Yate L., Saldívar-Guerra E., Ziolo R. F., (2016), The "Grafting-to" of well-defined polystyrene on graphene oxide via nitroxide-mediated polymerization. *Macromol. Chem. Phys.* 217: 2099-2106.
43. Ghavami Nejad A., Hashmi S., Joh H.-I., Lee S., Lee Y.-S., Vatankhah-Varnoosfaderani M., Stadler F. J., (2014), Network formation in graphene oxide composites with surface grafted PNIPAM chains in aqueous solution characterized by rheological experiments. *Phys. Chem. Chem. Phys.* 16: 8675-8685.
44. Varaprasad K., Jayaramudu T., Sadiku E. R., (2017), Removal of dye by carboxymethyl cellulose, acrylamide and graphene oxide via a free radical polymerization process. *Carbohyd. Polym.* 164: 186-194.
45. Che Man S. H., Mohd Yusof N. Y., Whittaker M. R., Thickett S. C., Zetterlund P. B., (2013), Influence of monomer type on miniemulsion polymerization systems stabilized by graphene oxide as sole surfactant. *J. Polym. Sci. Part A: Polym. Chem.* 51: 5153-5162.
46. Man S. C., Ly D., Whittaker M. R., Thickett S. C., Zetterlund P. B., (2014), Nano-sized graphene oxide as sole surfactant in miniemulsion polymerization for nanocomposite synthesis: Effect of pH and ionic strength. *Polymer.* 55: 3490-3497.
47. Fadil Y., Man S. C., Jasinski F., Minami H., Thickett S. C., Zetterlund P. B., (2017), Formation of homogeneous nanocomposite films at ambient temperature via miniemulsion polymerization using graphene oxide as surfactant. *J. Polym. Sci. Part A: Polym. Chem.* 55: 2289-2297.
48. Thomassin J.-M., Trifkovic M., Alkarmo W., Detrembleur C., Jérôme C., Macosko C., (2014), Poly(methyl methacrylate)/ Graphene Oxide Nanocomposites by a precipitation polymerization process and their dielectric and rheological characterization. *Macromol.* 47: 2149-2155.
49. Zhang H., Zhai D., He Y., (2014), Graphene oxide/ polyacrylamide/carboxymethyl cellulose sodium nanocomposite hydrogel with enhanced mechanical strength: Preparation, characterization and the swelling behavior. *RSC Adv.* 4: 44600-44609.
50. Huang Y., Zeng M., Ren J., Wang J., Fan L., Xu Q., (2012), Preparation and swelling properties of graphene oxide/ poly(acrylic acid-co-acrylamide) super-absorbent hydrogel nanocomposites. *Colloids and Surf. A: Physicochem. Eng. Asp.* 401: 97-106.
51. Liu P., Yao Z., Li L., Zhou J., (2014), In situ synthesis and mechanical, thermal properties of polyimide nanocomposite film by addition of functionalized graphene oxide. *Polym. Compos.* 37: 907-914.
52. Habib N. A., Chieng B. W., Mazlan N., Rashid U., Yunus R., Rashid S. A., (2017), Elastomeric nanocomposite based on exfoliated graphene oxide and its characteristics without vulcanization. *J. Nanomater.* 2017: 11.
53. Kazerouni S. S., Kalaee M., Sharif F., Mazinani S., (2016), Synthesis and characterization of poly(ethylene tetrasulfide)/graphene oxide nanocomposites by in situ polymerization method. *J. Sulf. Chem.* 37: 328-339.
54. Zhang C., Wang L., Zhai T., Wang X., Dan Y., Turng L. S., (2016), The surface grafting of graphene oxide with poly(ethylene glycol) as a reinforcement for poly(lactic acid) nanocomposite scaffolds for potential tissue engineering applications. *J. Mech. Behav. Biomed. Mater.* 53: 403-413.
55. Ren L., Liu T., Guo J., Guo S., Wang X., Wang W., (2010), A smart pH responsive graphene/polyacrylamide complex via noncovalent interaction. *Nanotechnol.* 21: 335701-335707.
56. Dimiev A. M., Tour J. M., (2014), Mechanism of graphene oxide formation. *ACS Nano*. 8: 3060-3068.
57. Bai H., Li C., Wang X., Shi G., (2011), On the gelation of graphene oxide. *J. Phys. Chem. C.* 115: 5545-5551.
58. Huang N. M., Lim H. N., Chia C. H., Yarmo M. A., Muhamad M. R., (2011), Simple room-temperature preparation of high-yield large-area graphene oxide. *Int. J. Nanomedic.* 6:

3443-3448.
59. Wei L., Wu F., Shi D., Hu C., Li X., Yuan W., Zhang Y., (2013), Spontaneous intercalation of long-chain alkyl ammonium into edge-selectively oxidized graphite to efficiently produce high-quality graphene. *Scientif. Rep.* 3: 2636-2642.
60. Cong H.-P., Wang P., Yu S.-H., (2013), Highly elastic and superstretchable graphene oxide/polyacrylamide hydrogels. *Small*. 10: 448-453.
61. Jeon I.-Y., Shin Y.-R., Sohn G.-J., Choi H.-J., Bae S.-Y., Mahmood J., Baek J.-B., (2012), Edge-carboxylated graphene nanosheets via ball milling. *Proceed. Nat. Acad. Sci. United States of Am.* 109: 5588-5593.
62. Emiru T. F., Ayele D. W., (2017), Controlled synthesis, characterization and reduction of graphene oxide: A convenient method for large scale production. *Egyp. J. Basic and Appl. Sci.* 4: 74-79.
63. Zhan D., Ni Z., Chen W., Sun L., Luo Z., Lai L., Shen Z., (2011), Electronic structure of graphite oxide and thermally reduced graphite oxide. *Carbon.* 49: 1362-1366.
64. Ganguly A., Sharma S., Papakonstantinou P., Hamilton J., (2011), Probing the thermal deoxygenation of graphene oxide using high-resolution in situ X-ray-based spectroscopies. *J. Phys. Chem. C.* 115: 17009-17019.
65. Claramunt S., Varea A., López-Díaz D., Velázquez M. M., Cornet A., Cirera A., (2015), The importance of interbands on the interpretation of the raman spectrum of graphene oxide. *J. Phys. Chem. C.* 119: 10123-10129.
66. López-Díaz D., López Holgado M., García-Fierro J. L., Velázquez M. M., (2017), Evolution of the raman spectrum with the chemical composition of graphene oxide. *J. Phys. Chem. C.* 121: 20489-20497.
67. Martins Ferreira E. H., Moutinho M. V. O., Stavale F., Lucchese M. M., Capaz R. B., Achete C. A., Jorio A., (2010), Evolution of theraman spectra from single-, few-, and many-layer graphene with increasing disorder. *Phys. Rev. B.* 82: 125429-125436.
68. Malard L. M., Pimenta M. A., Dresselhaus G., Dresselhaus M. S., (2009), Raman spectroscopy in graphene. *Phys. Rep.* 473: 51-58.
69. Wall M., (2012), Raman spectroscopy optimizes graphene characterization. *Adv. Mater. Proces.* 170: 35-38.
70. Liu R., Liang S., Tang X.-Z., Yan D., Li X., Yu Z.-Z., (2012), Tough and highly stretchable graphene oxide/polyacrylamide nanocomposite hydrogels. *J. Mater. Chem.* 22: 14160-14167.
71. Yu Y.-H., Lin Y.-Y., Lin C.-H., Chan C.-C., Huang Y.-C., (2014), High-performance polystyrene/graphene-based nanocomposites with excellent anti-corrosion properties. *Polym. Chem.* 5: 535-550.
72. Wan Y.-J., Tang L.-C., Gong L.-X., Yan D., Li Y.-B., Wu L.-B., Lai G.-Q., (2014), Grafting of epoxy chains onto graphene oxide for epoxy composites with improved mechanical and thermal properties. *Carbon.* 69: 467-480.
73. Rukmanikrishnan B., Sadhasivam B., Muthusamy S., (2016), Polytriazoleimide/graphene oxide nanocomposites and their properties. *Polym. Compos.* 39: 2202-2211.
74. Zhang N., Li R., Zhang L., Chen H., Wang W., Liu Y., Gao J., (2011), Actuator materials based on graphene oxide/polyacrylamide composite hydrogels prepared by in situ polymerization. *Soft Matter.* 7: 7231-7239.
75. Gao W., Alemany L. B., Ci L., Ajayan P. M., (2009), New insights into the structure and reduction of graphite oxide. *Nat. Chem.* 1: 403-408.
76. Ke Y., Wang Y., Ren L., Wu G., Xue W., (2010), Surface modification of PHBV films with different functional groups: Thermal properties and in vitro degradation. *J. Appl. Polym. Sci.* 118: 390-398.
77. Zhao X., Zhang Q., Hao Y., Li Y., Fang Y., Chen D., (2010), Alternate multilayer films of poly(vinyl alcohol) and exfoliated graphene oxide fabricated via a facial layer-by-layer assembly. *Macromolec.* 43: 9411-9416.
78. Song P., Cao Z., Cai Y., Zhao L., Fang Z., Fu S., (2011), Fabrication of exfoliated graphene-based polypropylene nanocomposites with enhanced mechanical and thermal properties. *Polymer*. 52: 4001-4010.
79. Alpaslan D., Ersen Dudu T., Aktas N., (2020), Synthesis of smart food packaging from poly(gelatin-co-dimethyl acrylamide)/citric acid-red apple peel extract. *Soft Mater.* 1-14.
80. Patole A. S., Patole S. P., Kang H., Yoo J.-B., Kim T.-H., Ahn J.-H., (2010), A facile approach to the fabrication of graphene/polystyrene nanocomposite by in situ microemulsion polymerization. *J. Colloid and Interf. Sci.* 350: 530-537.
81. Wilson D. I., (2017), What is rheology? *Eye*. 32: 179-186.
82. Wang X. W., Zhang C. A., Wang P. L., Zhao J., Zhang W., Ji J. H., Li X. P., (2012), Enhanced performance of biodegradable poly(butylene succinate)/graphene oxide nanocomposites via in situ polymerization. *Langmuir.* 28: 7091-7095.
83. Das S., Irin F., Ma L., Bhattacharia S. K., Hedden R. C., Green M. J., (2013), Rheology and morphology of pristine graphene/polyacrylamide gels. *ACS Appl. Mater. Interfac.* 5: 8633-8640.
84. Yang Y., Song S., Zhao Z., (2017), Graphene oxide (GO)/polyacrylamide (PAM) composite hydrogels as efficient cationic dye adsorbents. *Coll. Surf. A: Physicochem. Eng. Asp.* 513: 315-324.
85. Wang R., Wu L., Zhuo D., Zhang J., Zheng Y., (2018), Fabrication of polyamide 6 nanocomposite with improved thermal conductivity and mechanical properties via incorporation of low graphene content. *Indus. Eng. Chem. Res.* 57: 10967-10976.
86. Tseng I. H., Chang J. C., Huang S. L., Tsai M. H., (2013), Enhanced thermal conductivity and dimensional stability of flexible polyimide nanocomposite film by addition of functionalized graphene oxide. *Polym. Int*. 62: 827-835.